THE JOURNAL OF BIOLOGICAL CHEMISTRY VOL. 286, NO. 11, pp. 9405–9418, March 18, 2011

Nanomechanics of the Cadherin Ectodomain

*"CANALIZATION" BY Ca^{2+} BINDING RESULTS IN A NEW MECHANICAL ELEMENT**

Received for publication, July 30, 2010, and in revised form, December 13, 2010 Published, JBC Papers in Press, December 22, 2010, DOI 10.1074/jbc.M110.170399

Javier Oroz[‡1,2], Alejandro Valbuena[‡1], Andrés Manuel Vera[‡3], Jesús Mendieta[§¶], Paulino Gómez-Puertas[§], and Mariano Carrión-Vázquez[‡4]

From the [‡]Instituto Cajal/Consejo Superior de Investigaciones Científicas (CSIC), Centro de Investigación Biomédica en Red sobre Enfermedades Neurodegenerativas (CIBERNED), and Instituto Madrileño de Estudios Avanzados (IMDEA) Nanociencia, Avenida Doctor Arce 37, E-28002 Madrid, Spain, [§]Centro de Biología Molecular Severo Ochoa, CSIC-Universidad Autónoma de Madrid, E-28049 Madrid, Spain, and [¶]Biomol-Informatics SL, E-28049 Madrid, Spain

Cadherins form a large family of calcium-dependent cell-cell adhesion receptors involved in development, morphogenesis, synaptogenesis, differentiation, and carcinogenesis through signal mechanotransduction using an adaptor complex that connects them to the cytoskeleton. However, the molecular mechanisms underlying mechanotransduction through cadherins remain unknown, although their extracellular region (ectodomain) is thought to be critical in this process. By single molecule force spectroscopy, molecular dynamics simulations, and protein engineering, here we have directly examined the nanomechanics of the C-cadherin ectodomain and found it to be strongly dependent on the calcium concentration. In the presence of calcium, the ectodomain extends through a defined ("canalized") pathway that involves two mechanical resistance elements: a mechanical clamp from the cadherin domains and a novel mechanostable component from the interdomain calcium-binding regions ("calcium rivet") that is abolished by magnesium replacement and in a mutant intended to impede calcium coordination. By contrast, in the absence of calcium, the mechanical response of the ectodomain becomes largely "decanalized" and destabilized. The cadherin ectodomain may therefore behave as a calcium-switched "mechanical antenna" with very different mechanical responses depending on calcium concentration (which would affect its mechanical integrity and force transmission capability). The versatile mechanical design of the cadherin ectodomain and its dependence on extracellular calcium facilitate a variety of mechanical responses that, we hypothesize, could influence the various adhesive properties mediated by cadherins in tissue morphogenesis, synaptic plasticity, and disease. Our work represents the first step toward the mechanical characterization of the cadherin system, opening the door to understanding the mechanical bases of its mechanotransduction.

The acquisition of specific machinery for cell adhesion represented a crucial step in the evolution of metazoan organisms, enabling multicellularity and the development of tissues. There are four major classes of cell adhesion receptors: the immunoglobulin (Ig)-like superfamily, the cadherin superfamily, selectins, and integrins (1). Because of their location at the cell-cell interface, these receptors are often subject to mechanical stress (2, 3). However, to date only the mechanical properties of Ig and fibronectin type III domains have been investigated using atomic force microscopy (AFM)[5]-based single molecule force spectroscopy (SMFS) and protein engineering (4).

Cadherins can be defined (with some exceptions) as a superfamily of calcium (Ca^{2+})-dependent homophilic cell-cell adhesion proteins that mediate most cell adhesion in vertebrates, playing a crucial role in morphogenesis, synaptogenesis, tissue architecture, tissue repair, and carcinogenesis (5–7). Still, certain cadherins are heterophilic or/and connect two membranes from the same cell. At least in the case of the so-called "classical" cadherins (6, 8), their connection to the cytoskeleton appears to be mediated by several adaptor proteins (Refs. 9–11 and see Fig. 1*A*). This linkage is responsible for reinforcing cell-cell adhesion through a signaling pathway involving the activation of Rho, Rac, Cdc42, and the Arp2/3 actin nucleator complex (12–15). External mechanical stimuli are among the signals transduced by cadherins, which can induce changes in cell shape and synaptic plasticity (6, 16–19), triggering chemical or electrical (20) signaling. Furthermore, cadherin interactions are known to exert forces that have already been measured (21).

Classical cadherins are single pass transmembrane glycoproteins of 720–750 amino acids with an extracellular region (ectodomain or EC) that has a rodlike structure composed of five autonomously folded tandem domains (extracellular cadherin domains EC_1–EC_5 from the distal N terminus to the proximal C terminus; see Fig. 1, *A* and *B*). Although it is accepted that these cadherins establish homophilic interactions in *cis* and *trans* (22), the quaternary structure of these complexes remains unclear. The resolution of the atomic struc-

* This work was supported in part by grants from the Ministerio de Ciencia e Innovación, MICINN (Grant BIO2007-67116), Consejería de Educación de la Comunidad de Madrid, CECM (Grant S-0505/MAT/0283), and CSIC (Grant 200620F00) (to M. C.-V.) and from the MICINN (Grant SAF2007-61926), the CECM (Grant S-BIO-0260/2006-COMBACT), and the European Union (Grant FP7-223431) (to P. G.-P.).

[1] Both authors contributed equally to this work.
[2] Recipient of a fellowship from the CECM.
[3] Recipient of a fellowship from the Fundación Areces.
[4] To whom correspondence should be addressed. Tel.: 34-915854830; Fax: 34-915854754; E-mail: mcarrion@cajal.csic.es.

[5] The abbreviations used are: AFM, atomic force microscopy; SMFS, single molecule force spectroscopy; EC, ectodomain of cadherins; MD, molecular dynamics; SMD, steered MD; ΔL_c, increase in contour length; WLC, wormlike chain; TM, triple mutant; pN, piconewtons; r.m.s.d., root mean square deviation.

ture of the entire ectodomain of C-cadherin (a classical cadherin; Ref. 23) led to the proposal that *trans* interactions were based on a "β-strand-swapping" mechanism that only involved EC_1, whereas the *cis* interactions also involved EC_2. This model was consistent with electron microscopy data (24, 25) and fluorescence resonance energy transfer measurements (26). However, deletion analysis experiments (27, 28) and biophysical experiments using AFM (29), optical tweezers (30), and the surface force apparatus (31) showed that, although the model derived from the atomic structure of the ectodomain could be correct, it appears not to be exclusive as several interactions resulting from different degrees of overlap of the cadherin ectodomains are likely to occur. Indeed, the strongest interaction was detected with a complete overlap. Interestingly, recent evidence points to the existence of an intermediate binding conformation (termed "X-dimer"), which is necessary for the subsequent formation of the mature β-strand-swapping interaction (32, 33). Furthermore, non-classical cadherins seem to use a different mechanism of interaction (34–36).

The fact that cadherins transduce external mechanical stimuli (6, 16–20) makes the study of their nanomechanics a critical task as the first step toward understanding the underlying molecular mechanisms. To this end, unveiling the specific mechanical role of their ectodomain is essential. Related to this, the ectodomain has been postulated to function as a "force sensor" (37, 38), although the force sensitivity of cadherin junctions is still a matter of debate. Thus, in this context, it is highly relevant to study not only its intermolecular interactions (*i.e. cis* and *trans*, on which all nanomechanical studies of cadherins have focused so far; Refs. 29–32) but also the intramolecular interactions within the monomer. It is known that mature cadherin interactions are disrupted upon depletion of Ca^{2+} in the extracellular medium (5, 22), and indeed, cadherins were also proposed to function as "Ca^{2+} sensors" (39). Moreover, the cadherin ectodomain loses its rigidity and becomes a very flexible structure at low Ca^{2+} concentrations (40–44).

Our working hypothesis is that the nanomechanics of the monomeric cadherin ectodomain may change under different Ca^{2+} concentrations and that this differential response may affect the transduction of the mechanical signals within the cell. We have chosen C-cadherin as a study system as this is the only cadherin for which the atomic structure of the whole ectodomain is available.

C-cadherin is implicated in cell adhesion during the early stages of the development (*i.e.* the compaction of the morula) of *Xenopus laevis* (45, 46). This protein contains five EC domains, and each interdomain region can bind three Ca^{2+} ions such that the entire ectodomain is capable of binding 12 Ca^{2+} ions (Ref. 23 and see Fig. 1*B*). Ca^{2+} binding has a marked effect on the conformation of the protein as the binding of Ca^{2+} induces rigidity, whereas the unbound protein has a flexible structure (23, 40, 43, 44, 47). Although the role of Ca^{2+} in the structure and function of cadherins is well documented, to date no experimental data are available regarding the modulatory effects of Ca^{2+} binding on the nanomechanics of the ectodomain. This is particularly relevant given that these proteins are considered to act as mechanotransducers (3, 12–21, 37, 38, 48).

The cadherin fold, a compact unit with overall dimensions of $\sim 45 \times 25 \times 25$ Å in the presence of Ca^{2+}, is a Greek key fold with the N and C termini pointing toward opposite ends of the domain. This topology is remarkably similar to that of the Ig-like fold and superimposes quite well onto Ig I type ("intermediate"; Ref. 49), a class that includes the majority of Ig domains that are present in cell adhesion proteins, surface receptors, and muscle proteins (50). Both folds consist of seven β-strands with antiparallel pairings except for that between the A′ and G strands. These similarities are not likely to be the result of either sequence divergence or functional convergence but rather that of structural convergence (51). The nanomechanics of proteins with similar folds has previously been studied by AFM-based SMFS, revealing a relatively high mechanical stability for all of them (4). Here, using this technique and molecular dynamics (MD) simulations, we have directly measured the nanomechanical properties of the C-cadherin ectodomain and the effects of Ca^{2+} binding. We found that, upon Ca^{2+} binding, this structure rigidifies and "canalizes" its nanomechanical behavior, generating a novel mechanical element (the "Ca^{2+} rivet").

EXPERIMENTAL PROCEDURES

Expression and Purification of C-cadherin Ectodomain—The purified recombinant ectodomain of C-cadherin from *X. laevis* (UniProtKB/Swiss-Prot entry P33148) was provided by Dr. Barry Gumbiner (22). The protein was kept frozen (−80 °C) at ~0.5 mg/ml in 20 mM HEPES, 150 mM NaCl (pH 7.5) with either 1 mM $CaCl_2$ ("presence of Ca^{2+}") or 1 mM EGTA ("absence of Ca^{2+}").

Construction of Heteropolyproteins—To construct the heteropolyproteins containing the EC cadherin domains and the I27 marker domains (52), we used the only "ready-to-go" cloning/expression vector available (Ref. 53 and see Fig. 1*C*). A plasmid encoding the entire ectodomain of C-cadherin (22) was used as a template for the cloning of EC domains.

To construct the $(I27)_3$-EC_{1-5}-I27 polyprotein, the KpnI and MluI sites present in the I27-containing vector (53) were used as cloning sites. In the case of the $(I27)_3$-EC_{1-2}-$(I27)_2$ and $(I27)_3$-EC_2-$(I27)_2$ polyproteins, the KpnI and SpeI sites were selected for cloning. To construct the triple mutant (TM) D67A/D100A/D134A, the wild type EC_{1-2} sequence was cloned into the pT7blue vector (Novagen) using KpnI and SpeI sites prior to performing site-directed mutagenesis (one point mutation at a time) using the QuikChange kit (Stratagene). This construct was called EC_{1-2TM} and was cloned into the KpnI and SpeI sites of the aforementioned expression vector, which contains the I27 marker domains (53).

Domain boundaries were chosen according to those deposited in the Swiss-Prot Database (entry P33148) and in the Protein Data Bank (code 1l3w). The EC_{1-5} protein contained residues 1–540, EC_{1-2} residues 1–214, and the EC_2 domain residues 102–214 based on the sequence of the mature C-cadherin. All the sequences were verified by sequencing both strands of the DNA, and the cloning steps were carried out in the *Escherichia coli* XL1-Blue strain (Stratagene).

Expression and Purification of Heteropolyproteins—Heteropolyproteins were expressed in the *E. coli* C41(DE3) strain (54). Cells were grown at 37 °C to an A_{595} of 0.6–0.8 after which the expression of the recombinant heteropolyproteins was induced over 4 h by addition of 1 mM isopropyl β-D-1-thiogalactopyranoside. We determined the solubility of proteins by immunoblotting the soluble and insoluble fractions. The bacterial cells were lysed by treatment with 1 mg/ml lysozyme and 1% Triton X-100 as described previously (55).

Recombinant heteropolyproteins were purified by Ni^{2+} affinity chromatography using HisTrap HP FPLC columns (GE Healthcare) on an FPLC apparatus (ÄKTA Purifier, GE Healthcare) with a buffer containing 20 mM HEPES, 150 mM NaCl (pH 7.5), which was added with 50 mM imidazole for binding and 500 mM imidazole for elution. Either 1 mM $CaCl_2$ or 1 mM EGTA was added to the samples prior to the purification processes but not to the purification buffers (as recommended by GE Healthcare). Afterward, gel filtration purification was performed using a HiLoad 16/60 column (GE Healthcare) with a buffer containing 20 mM HEPES, 150 mM NaCl (pH 7.5) added with either 1 mM $CaCl_2$ or 1 mM EGTA (absence of Ca^{2+}). The concentrations of $CaCl_2$ and EGTA mentioned above were chosen on the basis of previous reports demonstrating that they saturated all the Ca^{2+} binding sites (40, 42, 43) or prevented C-cadherin interactions (22), respectively. The purified proteins were kept at ~0.5 mg/ml at 4 °C.

For the analysis of the $(I27)_3$-EC_{1-2}-$(I27)_2$ polyprotein in 0.1 mM $CaCl_2$, an aliquot of the polyprotein that was purified in the presence of 1 mM $CaCl_2$ was dialyzed extensively against a 20 mM HEPES, 150 mM NaCl (pH 7.5) buffer containing no added Ca^{2+}. Finally, several dialysis steps against a 20 mM HEPES, 150 mM NaCl, 0.1 mM $CaCl_2$ (pH 7.5) buffer were performed followed by concentration of the polyprotein sample in the same buffer by ultrafiltration using Amicon 10 K filters (Millipore). No Ca^{2+}/EGTA buffer was used to prepare this buffer based on the assumption that the residual Ca^{2+} concentration in Milli-Q water is in the low μM range (56).

To analyze the $(I27)_3$-EC_{1-2}-$(I27)_2$ polyprotein in the presence of magnesium ions (Mg^{2+}), we dialyzed an aliquot of the polyprotein (purified in the presence of EGTA) extensively against a 20 mM HEPES, 150 mM NaCl (pH 7.5) buffer containing neither EGTA nor Mg^{2+}. A final dialysis step against a 20 mM HEPES, 150 mM NaCl, 1 mM $MgCl_2$ (pH 7.5) buffer was performed followed by a dilution of the protein sample in the same buffer.

The concentration of each protein was estimated by spectrophotometry using its molar extinction coefficient. All the heteropolyproteins constructed using this method end with two C-terminal cysteine residues for their covalent attachment to the gold-coated coverslips used as AFM substrates. However, to avoid rupturing the disulfide bonds present in EC_5 (23), we only used reducing agents with $(I27)_3$-EC_{1-2}-$(I27)_2$ and $(I27)_3$-EC_2-$(I27)_2$ but not with the $(I27)_3$-EC_{1-5}-I27 polyproteins.

The heteropolyprotein $(I27)_3$-EC_{1-5}-I27 was highly insoluble, and only small amounts were obtained after purification, hindering the collection of sufficient data for statistical analysis. We also attempted to construct heteropolyproteins containing EC domains 4 and 5, $(I27)_3$-EC_{4-5}-$(I27)_2$, but encountered difficulties in their expression that rendered them unsuitable for AFM studies.

The expression of heteropolyproteins was performed in *E. coli*, whereas the expression of the entire ectodomain alone was performed in CHO cells (22). This difference provided us with an indication of the possible mechanical effects of glycosylation (the glycosylated domains are EC_2, EC_3, EC_4, and EC_5; Ref. 23). Our results suggest no significant differences in protein nanomechanics between the two expression systems.

Single Molecule Force Spectroscopy—We deposited ~2–20 μl of purified protein (at a concentration of 0.2–0.5 mg/ml) onto freshly evaporated gold-coated coverslips and allowed it to adsorb for ~10 min. The coverslips were rinsed with 20 mM HEPES, 150 mM NaCl (pH 7.5) containing either 1 mM $CaCl_2$ or 1 mM EGTA and then mounted in an atomic force microscope chamber for recording. We also carried out control experiments using either 5 mM $CaCl_2$ or 5 mM EGTA (or 1 mM EDTA) with the $(I27)_3$-EC_{1-2}-$(I27)_2$ polyprotein, obtaining data that were comparable with those obtained with 1 mM $CaCl_2$ or 1 mM EGTA, respectively (data not shown).

Our custom-made atomic force microscope and its mode of operation have been described previously (57). The spring constant of each individual atomic force microscope cantilever (Si_3N_4 tips, MLCT-AUNM, Veeco Metrology Group) was calibrated using the equipartition theorem (58), obtaining values that ranged from 35 to 70 $pN \cdot nm^{-1}$. Proteins were picked up by adsorption to the cantilever tip, which was pressed down onto the sample and then stretched for several hundred nm (Fig. 1*D*). All experiments were performed at a constant pulling speed of 0.4 $nm \cdot ms^{-1}$, and all the data were analyzed in Igor Pro 6 (Wavemetrics). The entropic elasticity of the stretched proteins was analyzed using the wormlike chain (WLC) model of polymer elasticity (59, 60),

$$F(x) = \frac{k_B T}{p}\left[\frac{1}{4(1 - x/L_c)^2} - \frac{1}{4} + \frac{x}{L_c}\right] \qquad \text{(Eq. 1)}$$

where F is the force, p is the persistence length, x is the end-to-end length, and L_c is the contour length of the stretched protein. L_c and p are the adjustable parameters.

Our criterion for unequivocal identification of single molecule recordings was the presence of four I27 force peaks in the case of the $(I27)_3$-EC_{1-5}-I27 polyprotein and at least four I27 peaks in the case of the $(I27)_3$-EC_{1-2}-$(I27)_2$ and $(I27)_3$-EC_2-$(I27)_2$ polyproteins as dictated by the geometry of the corresponding constructs in which four I27 events indicate that force was applied to the problem protein (Fig. 1*C*). The average F and ΔL_c values are reported with the S.E.

MD Simulations—The so-called generalized Born surface area approximation uses implicit solvent to simulate water molecules as a continuum with surface access corrections. We have recently demonstrated the validity of this approach in protein nanomechanics (57). We used the SANDER package from AMBER7 (61) suite programs and the parm-99 parameter set with the *effective Born radii* incorporated for Ca^{2+} ions (1.79 Å; Ref. 62). Starting from the Protein Data Bank coordi-

nates, we formulated the parameter files with LEaP software. The cysteine residues in EC_5 were bound, mimicking physiological conditions (23). A pairwise generalized Born model was used utilizing previously described parameters (63), and the surface areas were calculated using the linear combinations of pairwise overlaps model (64) with the default radii set up by LEaP. The time step along these simulations was 2 fs. The potential cutoff was fixed at 12 Å with a switching distance of 10 Å. After minimizing (with a time step of 1 fs) the initial structure with restrained Cα, the temperature was increased to 300 K, the restraints were then removed, and free molecular dynamics was performed over 10 ns. Different snapshots were selected every 2 ns as the starting points for the steered MD (SMD) simulations, which were carried out by imposing a restraint to both the N and C termini of the protein and increasing its length at a rate of 1 Å·ps^{-1} with a constant restraint force of 5 kcal·mol^{-1}·$Å^{-2}$. Ca^{2+} ions were also restrained (10 kcal·mol^{-1}·$Å^{-2}$) during the SMD to keep them included in the system. To avoid artifactual forces, these restraints were 0 for distances shorter than the linear distance between the coordinating residues.

All trajectories were loaded into VMD 1.8.6 (65), which was used to extract the N-C termini distance, backbone r.m.s.d., and dihedral angles. The dihedral angle is defined relative to three domains, and it is the angle between two planes, each one formed by two domains. We used Igor Pro 6 (Wavemetrics) to plot graphs and calculate the force exerted to the protein ($F = -k\cdot(NC_{measure} - NC_{restrain})$).

RESULTS

Nanomechanics of the Whole C-cadherin Ectodomain—To characterize the mechanical properties of the C-cadherin ectodomain (EC_{1-5}) at the single molecule level, the recombinant protein was adsorbed onto a gold-coated coverslip and placed into the recording chamber of an atomic force microscope. Random segments of the protein were picked up by the tip of the atomic force microscope cantilever and then stretched to analyze its nanomechanics at a pulling speed of 0.4 nm·ms^{-1} (Fig. 1*D*). As for other multimodular proteins previously studied (4), we obtained force extension recordings with a characteristic sawtooth pattern of similarly spaced force peaks (Fig. 2, *A* and *B*). Each force peak typically marks the unfolding of a domain, the amplitude of which indicates the mechanical stability (or unfolding force, *F*), whereas the spacing between consecutive peaks reflects the gain in length that results after domain unfolding (*i.e.* increase in contour length, ΔL_c, after fitting the peaks to the WLC).

We analyzed this protein in the presence of Ca^{2+} (1 mM $CaCl_2$) and in the absence of this ion (1 mM EGTA). In the presence of Ca^{2+}, the ectodomain behaves like a mechanostable protein, displaying several force peaks that we attribute to the unfolding of the different EC domains ($F = 186 \pm 4$ pN, $\Delta L_c = 34.2 \pm 0.1$ nm; $n = 252$; Fig. 2*A*). The structural differences among the EC domains in C-cadherin (23) are expected to contribute to some dispersion of ΔL_c. In the presence of EGTA, the force values fall drastically (83 ± 3 pN, $n = 119$; Fig. 2*B*), indicating that the Ca^{2+} coordination complexes, which are "extradomain" structural elements (Fig. 1*B*), can modulate the mechanical stability of the EC domains. It must be noted that the coordination complexes also contain residues that belong to the domains themselves as well as residues from the linker regions between domains. In addition to the force peaks produced by the unfolding of the EC domains, presumably resulting from the rupture of their mechanical clamps (4, 57), we were also able to detect several force peaks (143 ± 3 pN, $n = 128$) with ΔL_c values that are consistent with the disruption of the Ca^{2+} coordination complexes (2.7 ± 0.1 nm). We term this new mechanical element a Ca^{2+} rivet (Fig. 2, *A*, *C*, and *D*).

We could only observe up to four main force peaks because EC_5 is natively disulfide-bonded in a way that seems to reinforce its A′-G mechanical clamp (23), and therefore, it should not be unfolded in these experiments (because no reducing agent was used). Interestingly, the Ca^{2+} rivet always precedes the unfolding of an EC domain (showing lower forces than the latter). The ΔL_c values attributable to domain unfolding correspond very well with those expected for the folded domains, assuming a stretched length of 0.4 nm per amino acid (Ref. 66; the length of the force-hidden region after the mechanical clamp of the different ECs ranges from 81 to 88 amino acids, which would result in a nominal ΔL_c ranging from 32 to 35 nm approximately). In the absence of Ca^{2+}, no Ca^{2+} rivet is present, and the ΔL_c values were somehow randomly distributed, suggesting that the protein becomes less stable and that its unfolding pathway is less defined. Indeed, no correlation was observed in *F versus* ΔL_c scatter plots (data not shown). This is in accordance with previous thermal and chemical denaturation data from E-cadherin EC_{1-2} domains, which become very unstable in the absence of Ca^{2+}. This loss of stability is probably due to electrostatic repulsion effects resulting from the large number of negatively charged residues located in the regions between the EC domains (67, 68). In the presence of Ca^{2+} ions, this electrostatic repulsion is counterbalanced by the coordination of these ions. These considerations suggest that the extra force peaks observed experimentally originate from the forced disruption of the Ca^{2+} coordination complexes (the Ca^{2+} rivet). Furthermore, although the Ca^{2+} rivet may represent the rupture of residues that belong to the interdomain region and the domain itself, it seems to be both structurally and mechanically independent of the mechanical clamp of the EC domains. Although the modulation of the nanomechanics of a protein by ligand and ion binding has already been demonstrated (69–71), to our knowledge, this is the first time that ion binding has been shown to produce an autonomous mechanical feature.

We interpret our results in terms of a decrease in the number of mechanical unfolding pathways of the cadherin ectodomain in the presence of Ca^{2+}, a novel effect that we describe in terms of a "canalization" of the mechanical unfolding pathway. Thus, whereas in the presence of Ca^{2+} the mechanical unfolding pathway of the ectodomain is canalized into Ca^{2+} rivets and mechanical clamps of the EC domains (4, 57), in its absence, these pathways are numerous and variable, suggesting a "decanalization" effect on the energy landscape, which increases the number of mechanical pathways associated with a variety of barriers during the process of protein stretching.

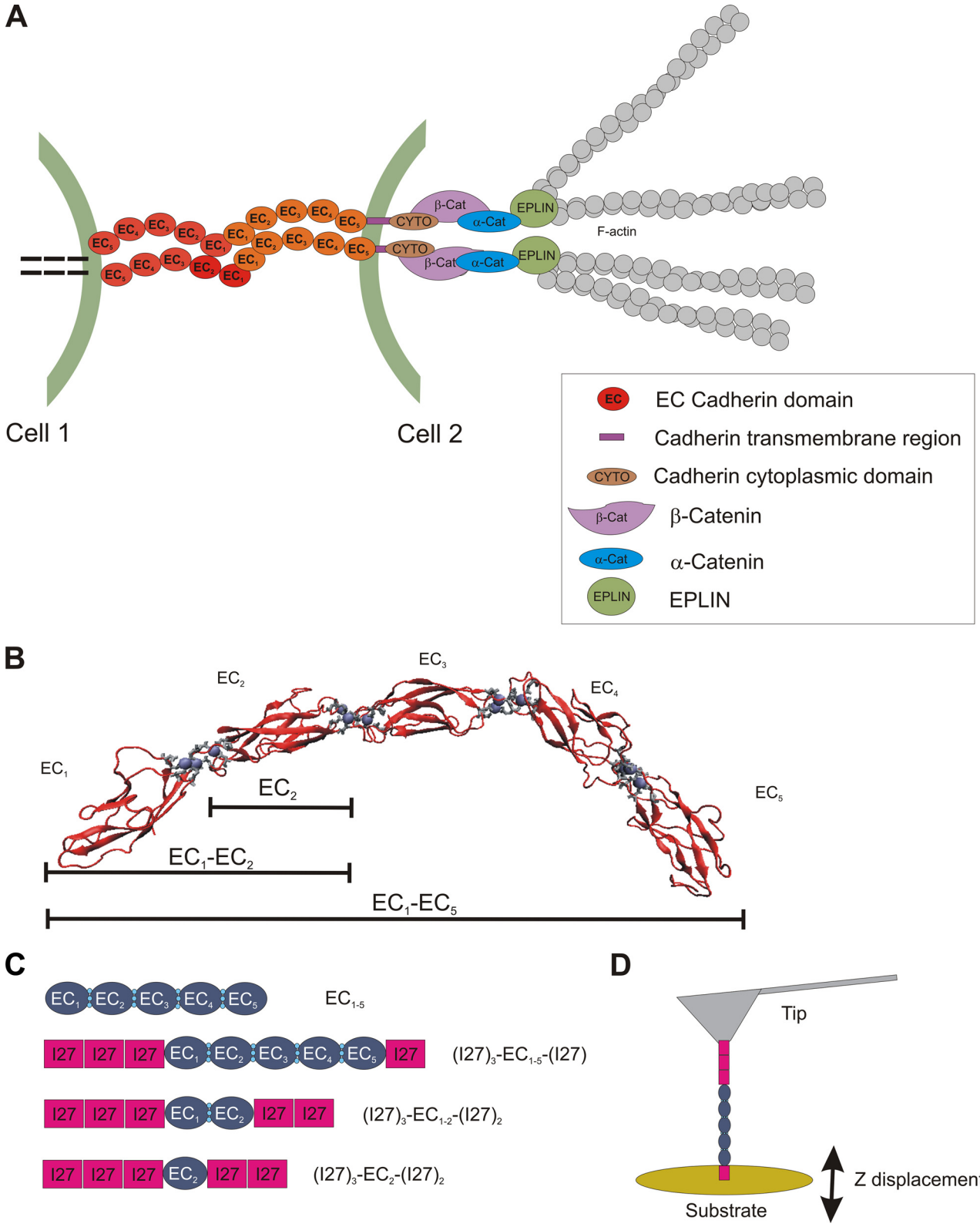

FIGURE 1. **Cadherin system and experimental setup.** *A*, classical cadherins are connected to the actin cytoskeleton through several adaptor proteins (9–11). Recent findings indicate that epithelial protein lost in neoplasm (EPLIN) appears to be the missing link connecting the system to the actin cytoskeleton (11). *B*, EC_1 (which contains the N terminus of the protein) is the cadherin domain most distal to the membrane, whereas EC_5 is the most proximal. Ca^{2+} ions (represented by *light blue spheres*) are bound in groups of three per interdomain region. The residues that form the coordination complexes (drawn in bond representation in VMD terminology; Ref. 65) not only belong to the linker between the EC domains but also to the domains themselves. The *bars* indicate the different protein regions included in our constructs. The structure of C-cadherin (Protein Data Bank code 1l3w) is represented by VMD 1.8.6 (65). *C*, scheme of the proteins and polyproteins analyzed in this study. *D*, schematic representation of an SMFS experiment. A drop of the sample is deposited on top of a substrate (a gold-coated coverslip) that can be moved in any direction with subnanometer resolution by a piezoelectric device (57). Through the movement of the piezoelectric device in the *z* axis, the substrate is moved up toward the tip so it can pick up a molecule and, upon retraction, stretch it.

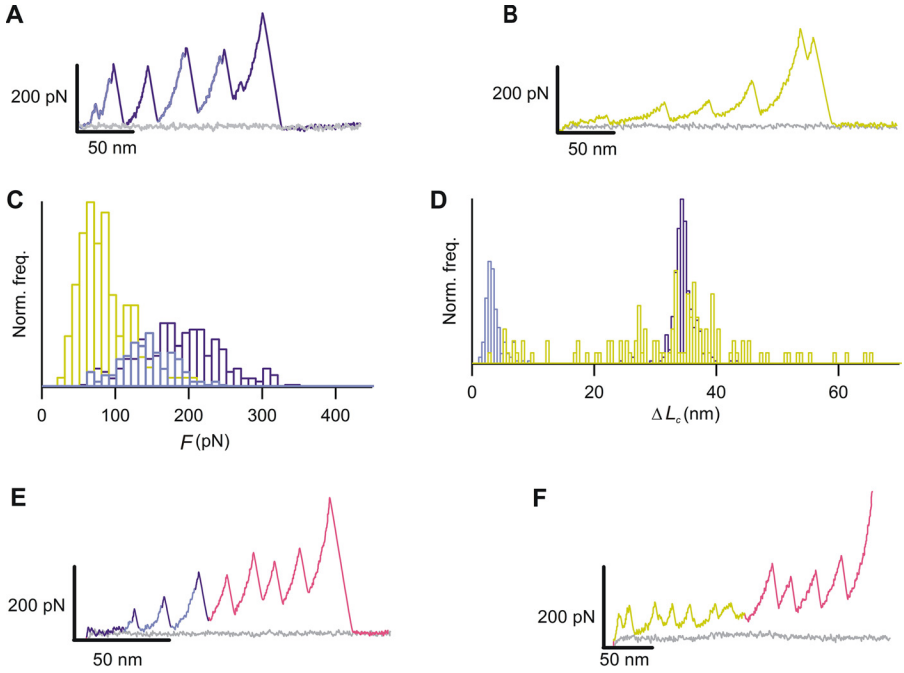

FIGURE 2. **Nanomechanics of the entire C-cadherin ectodomain.** *A* and *B*, typical SMFS recording of the entire C-cadherin ectodomain in 1 mM Ca^{2+} (*A*) and 1 mM EGTA (*B*). In the presence of Ca^{2+}, we observe several extra peaks or humps (*light blue*) identified as a deviation from the domain unfolding peak (*dark blue*; Ref. 4). Only the extra peaks or humps that precede domain unfolding peaks are included in our analysis. In the absence of Ca^{2+}, the extra peaks were never seen, and the magnitude of the forces was always lower than that in the presence of Ca^{2+}. Furthermore, the distance between peaks is not as well defined as in the presence of Ca^{2+}. This color code will be followed in the rest of the figures. *C*, force histograms showing that the forces are lower in the absence of Ca^{2+} (83 ± 3 pN) than in its presence (143 ± 3 pN for the extra peaks and 186 ± 4 pN for domain unfolding). *D*, ΔL_c histograms of the protein in the two conditions. In the presence of Ca^{2+}, the extra peaks show a mean value of 2.7 ± 0.1 nm, and the domain unfolding peaks show a mean value of 34.2 ± 0.1 nm. However, we cannot determine whether the extra peaks correspond to the rupture of individual coordination complexes or to the accumulation of several of them breaking simultaneously. In the absence of Ca^{2+}, there is a wide dispersion of the distribution. All histograms are normalized. *Norm. freq.*, normalized frequency. *E* and *F*, typical SMFS recordings of $(I27)_3$-EC_{1-5}-I27. In the presence of Ca^{2+} (*E*), this recording shows the same features as the ectodomain alone, displaying relatively high forces and extra peaks. We were unable to obtain recordings with more than three EC peaks. In the absence of Ca^{2+} (*F*), a fully undetermined pattern of ΔL_c and lower unfolding forces were observed.

To introduce a single molecule marker in our experiments, which allows us to unequivocally select single molecule recordings and disregard nonspecific interactions, multimers, aggregates, or other species present in the sample, we constructed heteropolyproteins with an internal marker of known mechanical stability (I27 domain of human cardiac titin; see "Experimental Procedures" and Fig. 1*C*). This strategy also provided us with an internal control to test the possibility that the chelating agent (EGTA) might also affect the mechanical stability of the marker. We found the same behavior of the cadherin EC domains in this construct, $(I27)_3$-EC_{1-5}-I27, as in the recombinant full-length ectodomain, and the I27 marker domains showed their typical mechanical pattern in both experimental conditions (Ref. 4 and see Fig. 2, *E* and *F*). However, this protein yielded only a few full-length recordings, which made it unsuitable for statistical analysis.

Nanomechanics of EC_{1-2}: Ca^{2+} Dependence, Mg^{2+} Replacement, and Site-directed Mutagenesis—To examine in detail these changes in the mechanical stability due to Ca^{2+} binding, we constructed an additional recombinant polyprotein containing a single set of Ca^{2+} binding sites located in the interdomain region (Fig. 1*C*). This protein contained EC domains 1 and 2 and one set of three Ca^{2+} binding sites: $(I27)_3$-EC_{1-2}-$(I27)_2$. We found mechanical properties in the ECs similar to those described for the entire ectodomain (Fig. 3). In 1 mM Ca^{2+}, we observed force peaks that presumably originated from the rupture of the Ca^{2+} coordination complexes (the Ca^{2+} rivet; $\Delta L_c = 3.0 \pm 0.2$ nm, $F = 90 \pm 5$ pN, $n = 26$), which preceded, sometimes as a "hump," one of the two main peaks that originated from the unfolding of the EC domains ($\Delta L_c = 34.6 \pm 0.2$ nm, $F = 102 \pm 5$ pN, $n = 50$; Fig. 3, *A–C*, *bottom*).

Using this polyprotein, we performed experiments in 0.1 mM Ca^{2+}, which is a Ca^{2+} concentration that, although still permitting residual cellular interactions (17), is not high enough to promote the conformational changes in classical cadherins that occur with 1 mM Ca^{2+} (Refs. 42 and 43 and see Fig. 3, *A–C*, *middle*). In this condition, the protein exhibited a decanalized unfolding pathway (without preferential ΔL_c values) with lower unfolding force values than those shown in 1 mM Ca^{2+} ($F = 81 \pm 7$ pN, $n = 69$) and no Ca^{2+} rivet. A very similar behavior was observed in the absence of Ca^{2+} (Fig. 3, *A–C*, *top*) where a decanalized unfolding pathway and low *F* values (84 ± 5 pN, $n = 66$) were found. For this construct, like the ectodomain in the absence of Ca^{2+}, no correlation was shown in *F versus* ΔL_c scatter plots for both the absence or presence of low Ca^{2+} concentration (data not shown). This confirms that, at low Ca^{2+} concentrations, the EC domains present an undefined unfolding pattern and become mechanically less stable.

We performed further studies with this polyprotein in the presence of Mg^{2+}, the divalent cation closest in size to Ca^{2+}.

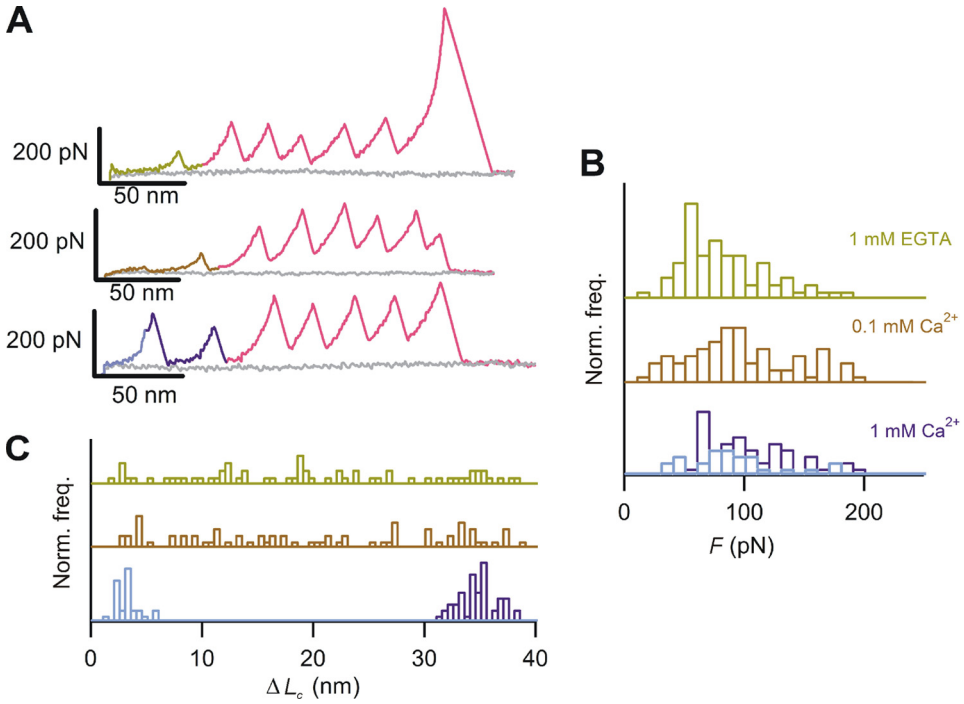

FIGURE 3. **Ca^{2+} effects on the nanomechanics of cadherin EC domains.** *A*, SMFS recording of the heteropolyprotein $(I27)_3$-$EC_{1,2}$-$(I27)_2$ in the absence and presence of 0.1 mM and 1 mM of Ca^{2+} (*top*, *middle*, and *bottom*, respectively). *B* and *C*, normalized histograms of *F* (*B*) and ΔL_c (*C*) in the aforementioned conditions. In 1 mM Ca^{2+}, the Ca^{2+} rivet shows an ΔL_c of 3.0 ± 0.2 nm. The domain unfolding distribution also shows an ΔL_c similar to that observed with the entire ectodomain (34.6 ± 0.2 nm). In the presence of 0.1 mM Ca^{2+}, the protein shows lower *F* values (81 ± 7 pN) than in 1 mM Ca^{2+} (90 ± 5 pN for the Ca^{2+} rivet and 102 ± 5 pN for the EC domain unfolding) and a high dispersion in the values of ΔL_c, indicating a decanalization of its mechanical unfolding pathway. No Ca^{2+} rivet was observed in these conditions. In the absence of Ca^{2+}, the protein behaved in a way similar to that in 0.1 mM Ca^{2+}: the ΔL_c values are largely undefined as if multiple unfolding pathways were possible (4), and the *F* histogram shows lower unfolding forces (84 ± 5 pN) than in the presence of 1 mM Ca^{2+}. *Norm. freq.*, normalized frequency.

In the presence of 1 mM Mg^{2+} (Fig. 4), two different classes of recordings were found: one with canalized domain unfolding (Fig. 4*A*, *right*; ΔL_c = 34.9 ± 0.1 nm, *F* = 72 ± 4 pN, *n* = 34) and the other with decanalized domain unfolding (Fig. 4*A*, *left*; *F* = 56 ± 5 pN, *n* = 48). However, we did not observe a putative "Mg^{2+} rivet." This is in agreement with previous results showing that at this concentration, Mg^{2+} binding is insufficient to promote the conformational changes seen in E-cadherin EC_{1-2} domains at the equivalent Ca^{2+} concentration (42), and it seems just to counterbalance the electrostatic repulsion effects, which can destabilize the EC domains. Considering that Mg^{2+} coordination is less thermodynamically stable than that of Ca^{2+} (42, 72), we interpret these results assuming that some of the ion binding sites occasionally bind Mg^{2+}, whereas others do not, remaining mechanically less stable. Indeed, the absence of Mg^{2+} rivets (Fig. 4*C*, *middle*) and the lower *F* values (compared with Ca^{2+}; Fig. 3*B*) observed in the canalized class (Fig. 4*B*) suggest that Mg^{2+} binding is less stable than that of Ca^{2+}.

To test our hypothesis that this new mechanical component (the Ca^{2+} rivet) is due to the rupture of the Ca^{2+} coordination complexes, we modified such complexes by site-directed mutagenesis to prevent ion coordination. Based on the crystallographic structure of the ectodomain (23), we constructed a TM in which three (of eight) negatively charged residues were replaced by alanine residues (D67A/D100A/D134A), which should prevent Ca^{2+} binding in between the EC_{1-2} domains (Fig. 5*A*). Accordingly, we expected that the Ca^{2+} rivet should be affected when this mutant protein is stretched in the presence of Ca^{2+}. Furthermore, as these mutations reduced the number of negatively charged residues in the linker region between the EC_{1-2} domains from eight to five, there would be a reduction in the possible electrostatic repulsion effect experienced in this region in the absence of Ca^{2+}. For nanomechanical analysis, we flanked this mutant with repeats of the I27 marker as in the wild type: $(I27)_3$-EC_{1-2TM}-$(I27)_2$ (Fig. 1*C*). Although we did not directly demonstrate that this protein could coordinate Ca^{2+}, a previous report on a single mutant that included one of the selected positions (D134A) showed it to be more sensitive to trypsin degradation and that it was unable to mediate adhesion, which was taken as indirect evidence that Ca^{2+} binding was disrupted in this mutant (73). No Ca^{2+} rivet was observed for this mutant protein in the presence of 1 mM Ca^{2+} (ΔL_c = 35.6 ± 0.5 nm, *n* = 44; Fig. 5, *B–D*, *bottom*). Interestingly, the magnitude of the force peaks that could be attributed to EC domain unfolding was slightly higher than that of the wild type protein (118 ± 11 pN). Furthermore, the ΔL_c for this mutant was slightly higher than that of the wild type. These differences may indicate that the perturbation of the conformation of the linker region in this mutant may also have slightly changed the mechanical clamp of the EC domains (4, 57). In the absence of Ca^{2+}, the nanomechanics of the domains was similar to that observed in its presence, showing comparable values (*F* = 120 ± 8 pN, ΔL_c = 35.6 ± 0.4 nm, *n* = 65; Fig. 5, *B–D*, *top*). Thus, the nanomechanics of this

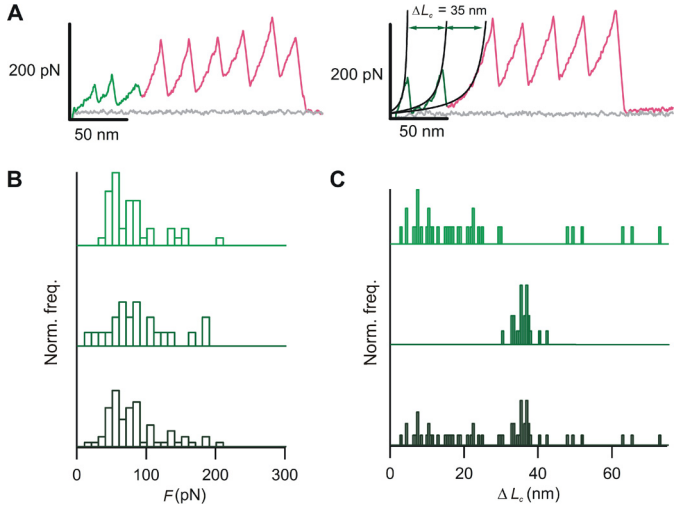

FIGURE 4. **Mg^{2+} effects on the nanomechanics of cadherin EC domains.** *A*, on the *left*, we show a recording of a molecule with low mechanical stability peaks and decanalized domain unfolding (*light green*; no fitting to a homogeneous family of WLC curves is possible here; Ref. 4), whereas on the *right*, we show a recording of a molecule with higher mechanical stability peaks and canalized domain unfolding (*dark green*; we show the fitting to the WLC). *B*, the *F* histograms show lower unfolding force values than those seen in the presence of Ca^{2+} (Fig. 3*B*). In the *bottom* distribution, all the force data are plotted ($n = 82$). The distribution in the *middle* shows the *F* for those molecules with canalized domain unfolding (*A*, *right*; 72 ± 4 pN), whereas that on the *top* shows the *F* for those with decanalized domain unfolding (*A*, *left*; 56 ± 5 pN). *C*, the corresponding ΔL_c histograms show that this protein can eventually be stabilized by Mg^{2+} coordination. The ΔL_c distribution of all the data from the EC domains under these conditions is shown at the *bottom*, demonstrating the two possible conformations (canalized and decanalized). The distribution in the *middle* shows the ΔL_c values for the mechanostable EC domains (*A*, *right*; 34.9 ± 0.1 nm). No Mg^{2+} rivets were seen here, meaning that the rupture of the Mg^{2+} coordination complexes was not stable enough to be resolved in our experiments. In the distribution on the *top*, we show the ΔL_c values resulting from the unfolding of the EC domains with decanalized unfolding (*A*, *left*). *Norm. freq.*, normalized frequency.

mutant was not sensitive to the presence of Ca^{2+}, and it did not show electrostatic repulsion effects in the linker region.

Nanomechanics of Single EC Domain—To examine the mechanical properties of a single EC domain in isolation without the linker region involved in Ca^{2+} binding, we constructed a polyprotein in which several I27 markers flanked the EC_2 domain: $(I27)_3$-EC_2-$(I27)_2$ (Fig. 1*C*). As expected, this domain behaved similarly in the presence or absence of Ca^{2+} (Fig. 6), and no Ca^{2+} rivet was found. The unfolding forces in the presence of Ca^{2+} were similar to those in its absence (88 ± 4 pN in Ca^{2+} and 82 ± 5 pN in EGTA, $n_{Ca^{2+}} = 24$, $n_{EGTA} = 25$). The ΔL_c values corresponded well with the size of the domain, considering that each stretched residue contributes 0.4 nm to the length (66): 35.2 ± 0.2 nm in Ca^{2+} and 34.9 ± 0.2 nm in EGTA. The expected size of the force-hidden region of the folded EC_2 domain is 87 amino acids, which represents 34.8 nm (87 × 0.4 nm), which is in close agreement with the results. Finally, these ΔL_c values were similar to those measured for the ECs in the other constructs studied. These results provide additional support to the proposal that the extra peaks observed in the presence of Ca^{2+} originate from an extradomain structure, *i.e.* the Ca^{2+} rivet.

SMD Simulations of the Whole Ectodomain—To access the atomic details of the structural changes taking place in the process, we performed MD simulations of the stretching of the entire ectodomain. Previous MD simulations focused on the rupture of the cadherin-cadherin interaction (74) and on the conformational changes that the ectodomain experiences upon Ca^{2+} binding (47, 75). Although several regions of the ectodomain have also been stretched from their termini by MD (35, 47, 76–78), the entire ectodomain has never been stretched before. Also, the extent of the stretching was somewhat short because of computational limitations. We performed our analysis using the generalized Born surface area approximation as described previously (57). This approach allowed us to run 10 ns of free MD and to perform five stretching simulations of the entire ectodomain at larger extensions, which allowed us to stretch all the domains. Similar to previous results (47), we observed much larger fluctuations in the entire ectodomain in the absence of Ca^{2+} with the fold of the individual EC domains remaining intact (Fig. 7, *A* and *B*). EC_5 still showed more backbone deviation in the absence of Ca^{2+} than the other domains. These results confirm the rigidification effect experienced by the cadherin ectodomain upon Ca^{2+} binding (40–44, 47, 75). We also monitored the dihedral angles between domains during all free MD simulations (see "Experimental Procedures" and Fig. 7, *C* and *D*). Interestingly, Ca^{2+} binding triggered very different effects in different regions of the ectodomain. In the presence of Ca^{2+}, the EC_{123} angle was around 90° (varying from 27° to 137°), whereas the EC_{345} angle was around 180° (with a minimum of 126°). In the absence of Ca^{2+}, the angle became about 180° for EC_{123} (fluctuating from 140° to 180°), and it fluctuated highly for EC_{234} and EC_{345} (varying from 27° to 172° and from 59° to 175°, respectively). These results suggest a switching mechanism in which the presence of Ca^{2+} rotates the distal region of the ectodomain and aligns the proximal region, whereas in its absence, the distal region remains aligned, and the proximal region becomes more motile.

Before addressing the atomic details of the stretching process, an obvious prerequisite is that the simulations should correlate with our experimental observations. Indeed, the simulations of the stretching of the ectodomain closely reproduced the experimental results qualitatively both in the presence and absence of Ca^{2+} (Fig. 8, *A*–*D*). In the presence of Ca^{2+}, we observed extra peaks (*i.e.* putative Ca^{2+} rivets) that could be attributed to the rupture of the different Ca^{2+}-binding complexes. The criterion we used to assign Ca^{2+}-related events was to monitor the release of Ca^{2+} ions and correlate it to the location of events in the curve (Fig. 8*A*). Although we could not identify specific force peaks *a priori* as Ca^{2+} rivets (by just observing the curve) as they were often masked in the noise, we could assign them by using the above criterion. In Fig. 8*A*, we only marked as extra peaks those that could be assigned unambiguously. Only four unfolding peaks were observed because in the simulations we maintained the disulfide bonds that are natively formed in EC_5 and covalently lock its putative A′-G mechanical clamp (23). We observed that most of the time these Ca^{2+} rivets correlated with immediate domain unfolding, similar to the SMFS experiments. In contrast, we detected several EC unfolding intermediates in this condition (Fig. 8, *A* and *E*) that were not observed in the experi-

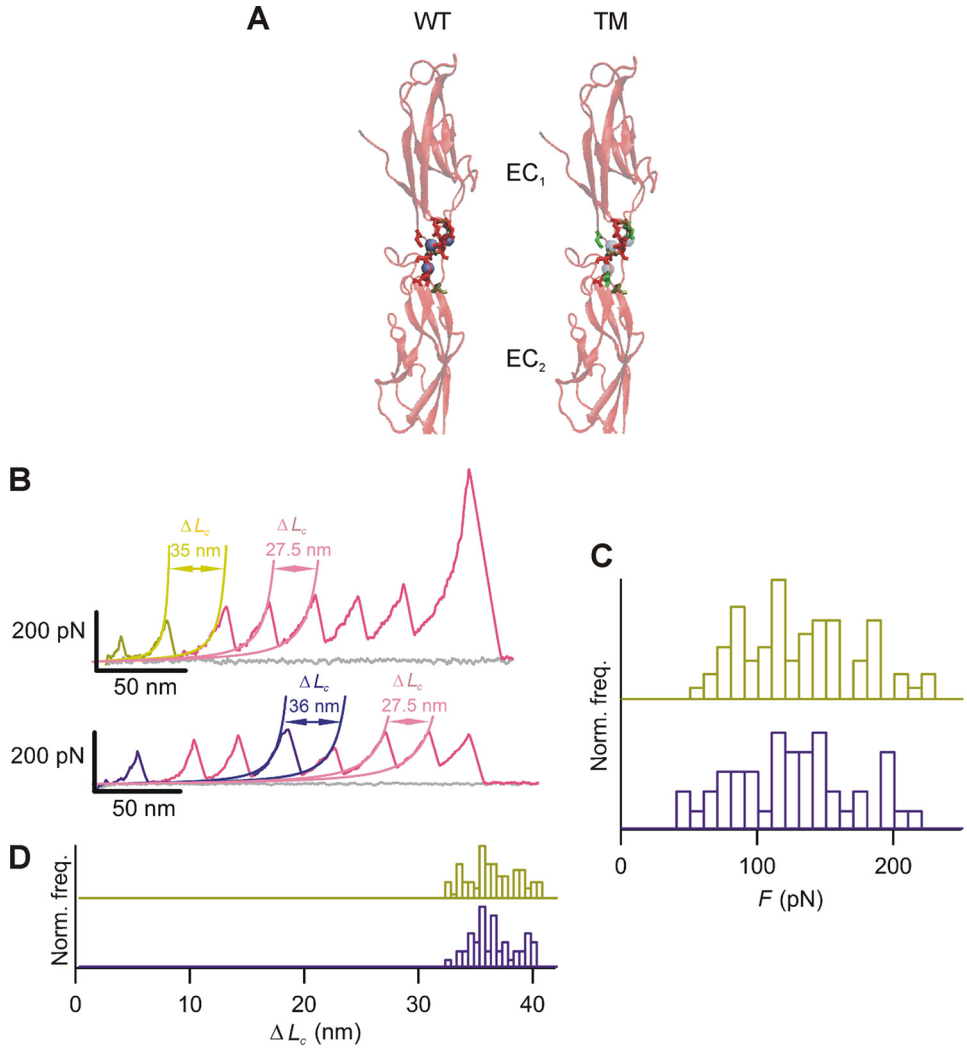

FIGURE 5. **Triple EC mutant shows no mechanical dependence on Ca^{2+} binding.** *A*, on the *left*, the wild type (WT) shows the negatively charged residues from the coordination complexes in *red* (Glu-11, Asp-67, Glu-69, Asp-100, Asp-103, Asp-134, Asp-136, and Asp-195), the rest of the residues in *brown*, and the Ca^{2+} ions as *blue spheres*. In the TM (D67A/D100A/D134A; *right*), the three mutated residues are highlighted in *green*, showing that each point mutation affects a single coordination complex (Ca^{2+} ions are represented here as *transparent blue spheres*). The structures are displayed by VMD 1.8.6 (65). The structure of the domains is represented in transparent "new cartoon" in VMD terminology (Protein Data Bank code 1I3w). The residues that form the coordination complexes are drawn in bond representation. *B*, SMFS recording of the heteropolyprotein $(I27)_3$-$EC_{1,2TM}$-$(I27)_2$ in the presence and absence of Ca^{2+} (*bottom* and *top*, respectively). No Ca^{2+} rivet is present in this protein in any condition. We show the fitting of the force peaks to the WLC model, which allows us to identify the different domains of the polyprotein marker (in *pink*) and characterize the domains under study. *C*, the *F* histograms are similar in Ca^{2+} (*bottom*) and non-Ca^{2+} (*top*) conditions (118 ± 11 and 120 ± 8 pN, respectively). *D*, the ΔL_c histograms for this protein show similar distributions in both conditions (35.6 ± 0.5 nm for Ca^{2+} and 35.6 ± 0.4 nm for EGTA), indicating that Ca^{2+} binding has no effect in the mechanical stability of this mutant protein. *Norm. freq.*, normalized frequency.

ments. This difference may result from the different pulling speeds used in each method (simulations were done at 1 Å·ps^{-1}, 8 orders of magnitude faster than the AFM experiments that are performed at 0.4 nm·ms^{-1}). In the absence of Ca^{2+}, as in the experiments, the unfolding forces were lower, whereas the ΔL_c values did not follow any preferential unfolding pathway, remaining decanalized (Fig. 8*B*). Also, the unfolding hierarchy of the domains seems to be less well defined (Fig. 8, *E* and *F*).

Finally, we should note that our pulling simulations were in close agreement with previous simulations of specific cadherin domains (35, 47, 77, 78), which also predicted force peaks originating from the rupture of the Ca^{2+} coordination complexes (Ca^{2+} rivets) and higher unfolding forces for the EC domains than those seen in the absence of Ca^{2+}. However, none of these studies reported the mechanical canalization we have shown in the presence of Ca^{2+}, probably due to the fact that those simulations only examined a single domain rather than the complete ectodomain.

DISCUSSION

Taken together, our findings led us to conclude that the cadherin ectodomain is a mechanostable structure highly dependent on the Ca^{2+} concentration. In the absence of Ca^{2+}, its mechanical unfolding pathway appears to be decanalized, whereas in the presence of Ca^{2+}, we observed a canalized unfolding pathway showing domain unfolding preceded by specific Ca^{2+} rupture events (Fig. 9*A*). Although the influence of Ca^{2+} on the structure, conformation, and function of cadherins is well documented, the role of Ca^{2+} as a mechanical

stabilizer of these proteins has not been experimentally demonstrated before. Here we present the first evidence that the nanomechanics of these proteins is strongly dependent on Ca^{2+} binding. Therefore, the ectodomain behaves as a "Ca^{2+}-sensitive" mechanostable structure. Furthermore, we have discovered a novel element of mechanical resistance in proteins comprising an ion coordination complex, which behaves as an "interdomain" clamp: the Ca^{2+} rivet. Hence, we demonstrate that Ca^{2+} ions have two different effects: they provide EC domains themselves with defined mechanical resistance such that they show true mechanical clamps (*i.e.* modularly autonomous resistance elements), and they generate extradomain mechanical resistance elements that seem to protect the mechanical clamps.

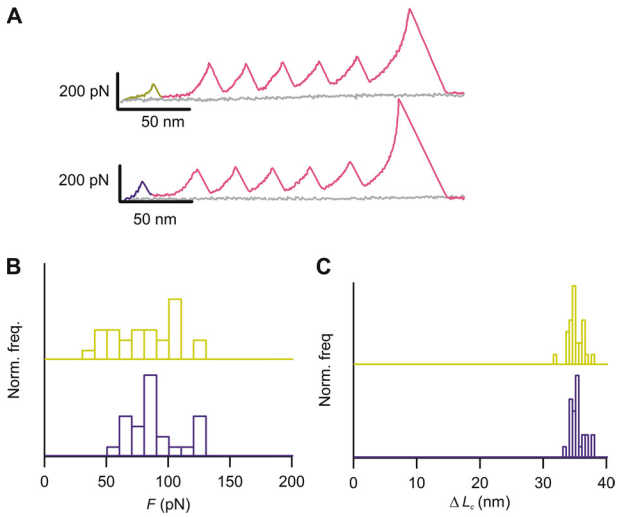

FIGURE 6. **Nanomechanics of single EC domain is not affected by Ca^{2+} binding.** *A*, SMFS recordings of $(I27)_3$-EC_2-$(I27)_2$ in the absence (*top*) and the presence (*bottom*) of Ca^{2+}. The presence of Ca^{2+} has no effect on the modulation of the mechanical stability of an EC domain presumably because the Ca^{2+} coordination complex cannot be formed. *B* and *C*, normalized histograms of *F* (*B*) and ΔL_c (*C*) for EC_2. Both histograms of *F* (82 ± 5 pN for EGTA and 88 ± 4 pN for Ca^{2+}, *top* and *bottom*, respectively) and of ΔL_c (34.9 ± 0.2 nm for EGTA and 35.2 ± 0.2 nm for Ca^{2+}) are comparable. The presence of Ca^{2+} does not directly alter the mechanical stability of the cadherin domain *per se* but rather through the electrostatic neutralization of the Ca^{2+} coordination region. It can be concluded that the mechanical stability of an individual EC domain does not depend on Ca^{2+}, which acts as a mechanical stabilizing element of the ectodomain. *Norm. freq.*, normalized frequency.

Based on our findings (*i.e.* the ectodomain as a Ca^{2+}-dependent mechanostable structure) and considering that residual adhesion in low Ca^{2+} concentration has already been reported (17, 29), we postulate that the ectodomain behaves as a "Ca^{2+} switch" in which Ca^{2+} binding determines its nanomechanical properties, including its mechanical integrity. The biological relevance of our findings can be fully appreciated considering that the local concentration of extracellular Ca^{2+} in specific microenvironments varies widely during development and adulthood in many physiological processes (48, 79–82). For instance, after electrical depolarization of the synapse, it is known that the Ca^{2+} levels in the synaptic cleft can drop from basal levels (around 1–2 mM) to 0.1 mM (48, 83). Interestingly, considering that these changes are not expected to completely abolish cadherin adhesion (17, 84) and that cadherin has been proposed as a physiological reader (*i.e.* sensor) of external Ca^{2+} fluctuations (39), the mechanical response of the ectodomain to Ca^{2+} changes clearly appears to be critical (Fig. 9, *B* and *C*).

We have shown here that in the absence of Ca^{2+} the ectodomain displays higher conformational plasticity than in its presence, which not only dramatically affects its conformation but also its mechanical behavior. This would in turn determine the way it transmits mechanical stimuli (Fig. 9, *B* and *C*). Considering that the Ca^{2+} binding sites in the ectodomain are not equivalent and that the range of their affinity constants is rather large (40–43), the possibility of the existence of differential mechanical properties along the ectodomain remains to

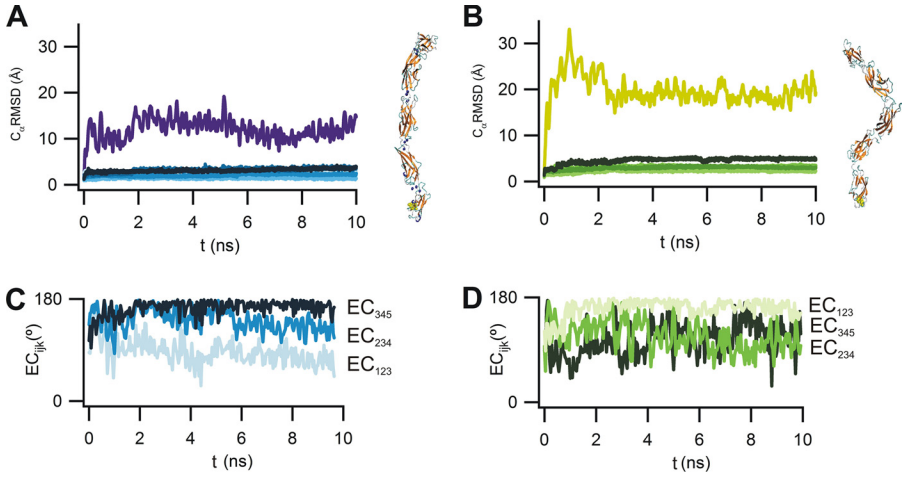

FIGURE 7. **Free MD simulations of C-cadherin ectodomain.** *A* and *B*, r.m.s.d. of the C-cadherin ectodomain in the presence (*A*) or absence (*B*) of Ca^{2+} during 10 ns of free MD. At the *bottom* of the graphs, we show the r.m.s.d. of the individual domains, the most distal to the membrane represented in *lighter colors* (this color code will be maintained in the rest of the panels of this figure and in Fig. 8). The structure of the individual domains is preserved in both conditions (with slightly larger deviations in the absence of Ca^{2+}) with an r.m.s.d. in the range of 1–3.5 Å with Ca^{2+} and 2–5 Å without Ca^{2+}. The tertiary structure of the ectodomain in the absence of Ca^{2+} shows much larger deviations in the r.m.s.d. (values up to 18 Å) than in its presence (r.m.s.d. close to 12 Å), indicating a greater flexibility of the structure in these conditions. *C*, dihedral angles during the free MD in the presence of Ca^{2+}. The proximal region (close to the membrane) of the ectodomain remains aligned (~180°) during the 10 ns of free MD, whereas the distal region rotates 90°. *D*, dihedral angles in the absence of Ca^{2+}. In these conditions, the evolution of the free MD is completely different with the more distal region (EC_{123}) aligned, whereas the more proximal dihedral angles (EC_{234} and EC_{345}) display a stochastic behavior.

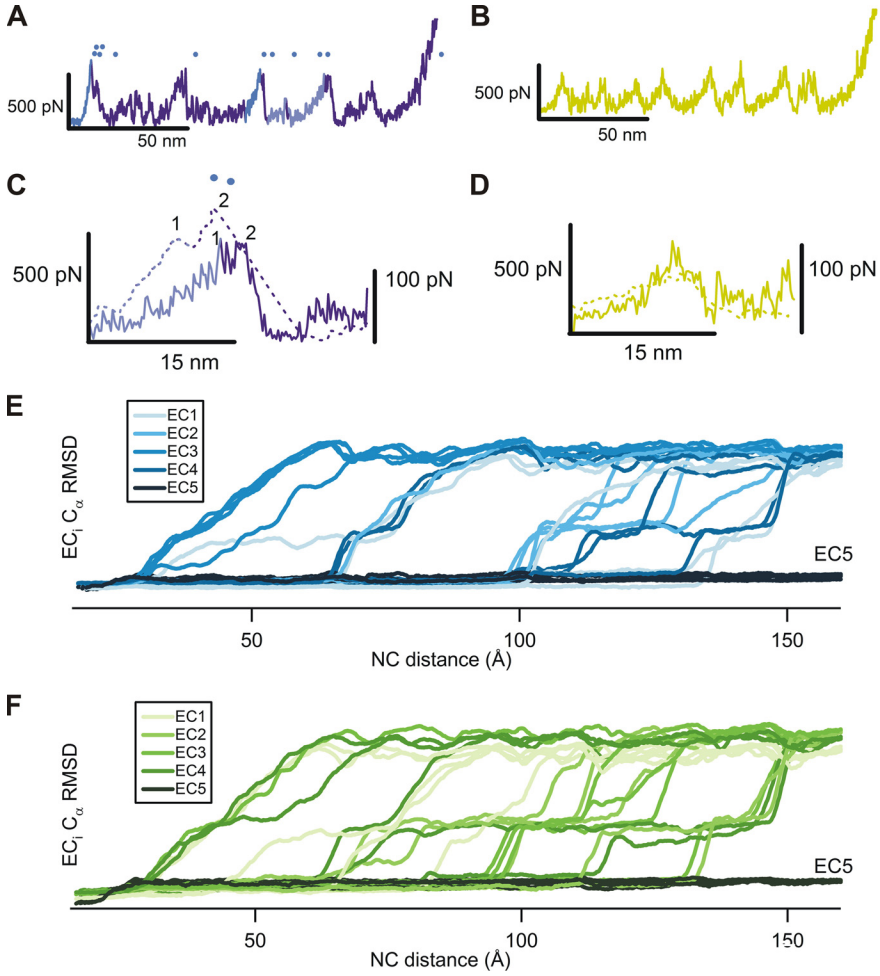

FIGURE 8. **SMD of the whole C-Cadherin ectodomain.** *A*, SMD of the complete ectodomain from the Cα of the N and C termini in the presence of Ca^{2+}. Force peaks range from 260 to 560 pN. Peaks associated with the rupture of the Ca^{2+} coordination complexes are shown in *light blue*, whereas those associated with the unfolding of the EC domains are colored *dark blue*. The ion release (*light blue spots*) comes several ps after the appearance of the force peak due to the rupture of the corresponding Ca^{2+} coordination complex. The ΔL_c between the force peaks ranges from 30 to 37 nm. Furthermore, several EC unfolding intermediates were evident in these simulations that were not observed in the experimental recordings. *B*, SMD of the complete ectodomain from the Cα of the N and C termini in the absence of Ca^{2+}. Force peaks range from 220 to 450 pN, whereas the ΔL_c values range from 8 to 25 nm. *C* and *D*, superimposition of experiments and simulations in the presence (*C*) or absence (*D*) of Ca^{2+}. In *C*, the first peak from Fig. 2*A* (*dashed line*) and the fourth peak from *A* (*continuous line*) are shown. The simulations show the distortion and rupture of the Ca^{2+} coordination complexes of two Ca^{2+} ions (number *1*; shown in *light blue*), which precede the unfolding of the EC domain (number *2*). This coincides well with the extra peak seen in the experiment (with a ΔL_c of 3.5 nm; measured until the EC unfolding peak). The two graphs are equalized. The simulation scale is on the *left side*, and the experimental scale is on the *right side*. In *D*, the first peak from Fig. 2*B* (*dashed line*) and the first peak from *B* (*continuous line*) are shown. In both cases, the magnitude of the forces are lower than in the presence of Ca^{2+} (*C*). *E* and *F*, backbone r.m.s.d. of the individual domains in the presence (*E*) or absence (*F*) of Ca^{2+} during the five SMD simulations that were performed. In *E*, the EC_3 domain is the first to unfold in all the SMD simulations performed. In *F*, there is an increased heterogeneity in the hierarchy of domain unfolding. Thus, the unfolding of the ectodomain in the absence of Ca^{2+} displays a more stochastic behavior than in the presence of Ca^{2+}, which appears to canalize this response. The plateaus seen in both graphs represent several EC unfolding intermediates that were not observed in the AFM experiments.

be explored. This heterogeneity would add an additional layer of complexity to the proposed role in force transmission.

It is known that when extracellular levels of Ca^{2+} are depleted, mature cadherin homophilic interactions are disrupted (5, 22). However, recent evidence demonstrates that a local and temporal depletion in extracellular Ca^{2+} levels does not necessarily imply a complete disruption of cellular adhesion. This could later facilitate plastic rearrangements in the cell junctions (17, 18, 32, 33, 39, 48, 84). Thus, certain Ca^{2+} concentrations may still allow the cadherin-cadherin interaction to occur while affecting some mechanical properties of the ectodomain. Such an effect would alter the manner in which it transmits mechanical signals (Fig. 9, *B* and *C*) and may in turn affect the strength of the adhesion contact. Indeed, the unfolding of protein domains may not only regulate the range but also the life span of a single adhesion bond, acting as a molecular "shock absorber" (85, 86). It is also of interest to test whether the Ca^{2+} rivet, the new element of resistance described here, appears during the stretching of a single cadherin-cadherin complex. This type of experiment is hard to implement but would allow us to build a more complete mechanical picture of the system so we can begin to understand how these mechanical signals are transduced through the cadherin-catenin system, promoting different cell responses.

To establish the biological relevance of the ectodomain nanomechanics in cell-cell adhesion and mechanotransduction, it is critical to compare the mechanical properties of the

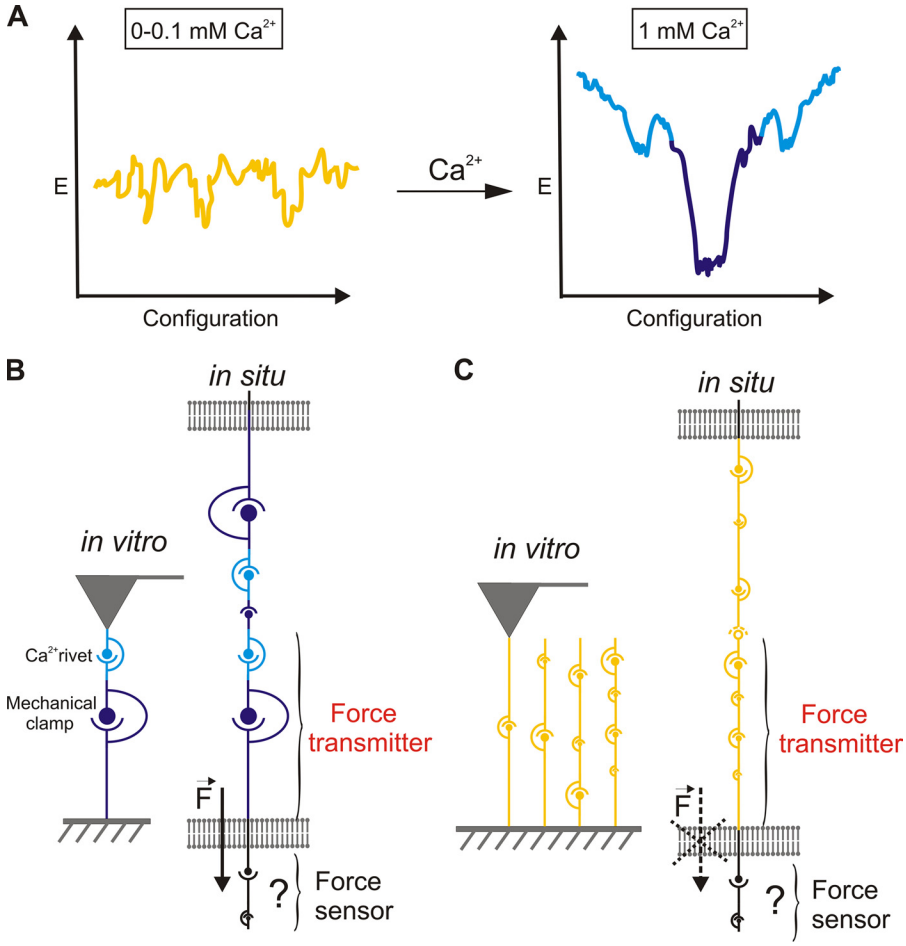

FIGURE 9. **Nanomechanics of the ectodomain and the Ca^{2+} switch hypothesis.** *A*, diagram showing the mechanical folding energy (*E*) landscape of an EC domain in low and high Ca^{2+} concentration. At high Ca^{2+} concentrations, the mechanical unfolding of an EC domain is trapped into two energy minima: that of the Ca^{2+} rivet and that of the mechanical clamp of the domain. Landscapes are represented schematically in a one-dimensional cross-section. The color code is the same used in the rest of the figures. *B*, a high Ca^{2+} concentration rigidifies and canalizes the unfolding pathway of the ectodomain and adds a novel mechanical component (the Ca^{2+} rivet). This structure may therefore act as a rigid force transmitter (*i.e.* without significant force damping). *C*, a low Ca^{2+} concentration decanalizes and destabilizes the ectodomain, also removing the Ca^{2+} rivet. This may allow for structural rearrangements, which should in turn affect the force transduction mechanism. Our results suggest that the cadherin ectodomain may be the force transmitter of the system, whereas the actual force sensor may be an intracellular component of the cadherin system (analogous to the talin rod in the integrin system; Refs. 38, 48, 89, and 90)[6] whose mechanical properties are still to be determined (represented by *question marks*).

ectodomain with the mechanical strength of the cadherin-cadherin interaction. Although the latter has not yet been unequivocally measured (*i.e.* using single bond markers), a previous report estimated this strength *in vitro* to be ~40 pN (at a comparable pulling speed; Ref. 29). Furthermore, several experiments on live cells showed comparable rupture values for single cadherin interactions, although these measurements were strongly dependent on the catenin-actin system, which could alter the force of the interaction through unknown conformational effects on the cadherin system triggered from inside the cell (12–15, 17, 87, 88). The magnitude of these rupture forces is clearly below that of both Ca^{2+} rivets and EC mechanical clamps in the presence of Ca^{2+}. This may imply that the cadherin ectodomain is not the "force-sensing" element of the cadherin-catenin system (Fig. 9, *B* and *C*).

In summary, the ectodomain can show two extreme mechanical behaviors: (i) a fairly rigid and stable structure, the integrity of which would assure the adequate transmission of mechanical stimuli (at high Ca^{2+} concentrations) and (ii) a compliant structure that may affect the mechanical transmission (at low Ca^{2+} concentrations). Thus, the force sensor of the system should be another component with a mechanical stability below the magnitude of adhesion forces mentioned above (working on the range of up to ~40 pN; Fig. 9, *B* and *C*). Both β- (48)[6] or α-catenin (38) seem to be better candidates for being the force-sensing elements of this system in a manner analogous to that of the talin rod in the integrin system, the mechanical stability of which is below 50 pN at a comparable loading rate (90).

Our hypothesis of the Ca^{2+} switch would only be valid if residual adhesion is present in the system at low Ca^{2+} concentrations. Otherwise, adhesion would be impaired, and the mechanical properties of the ectodomain would be physiologically irrelevant (*i.e.* a mere epiphenomenon). If this were the case, the mechanical properties of the ectodomain at high Ca^{2+} concentrations would represent the only properties physiologi-

[6] A. Valbuena, A. M. Vera, J. Oroz, M. Menéndez, and M. Carrión-Vázquez, manuscript under review.

cally relevant as they would assure the integrity of the structure and the adequate transmission of mechanical signals.

This hypothesis and that of the shock absorber effect of the ectodomain (85, 86) could be tested in the future by *in vitro* SMFS experiments using an unequivocal design to measure the interaction in whole ectodomains (*i.e.* by measuring the relationship between the mechanical stability and lifetime of this interaction with the compliance of the ectodomain). Furthermore, SMFS experiments with cells (87) in which the Ca^{2+} concentration is varied could also provide valuable information in this regard. However, in both cases, a single bond marker should first be developed for unambiguous analysis. Nevertheless, our results represent an important first step required for the interpretation of future experiments of this type.

Future experiments should also explore intermediate concentrations of Ca^{2+} to determine whether the "all-or-none" behavior we report here (1 *versus* 0.1 mM or sub-μM Ca^{2+}) represents the whole picture or whether a gradual response is rather present.

Furthermore, it is interesting to note that a number of mutations in the cadherin ectodomain that do not affect the cadherin-cadherin interaction have been described in relation to pathologies, including several gastric cancers (7) as well as familial deafness and the Usher syndrome (20, 35, 91–93). These diseases may well be hypomorphic mutations affecting the mechanical stability of the cadherin EC domains, which would affect in turn the manner in which the ectodomain transmits forces. This has in fact been postulated for some of these disorders (Ref. 93 and see Fig. 9, *B* and *C*). In addition, some of these mutations are directly related to the Ca^{2+} rivet, the new mechanical element described in this study (35, 91, 92). This highlights the relevance of studying the nanomechanics of the ectodomain and, in particular, the potential importance of the Ca^{2+} rivet. Finally, we propose that the versatile mechanical design of the cadherin ectodomain and its dependence on Ca^{2+} concentration may allow for a variety of mechanical responses that could mediate the various adhesive properties that cadherins display during tissue morphogenesis, synaptic plasticity (in development and adulthood), and tumor metastasis.

Acknowledgments—We thank B. Gumbiner (University of Virginia, Charlottesville, VA) for kindly providing both the C-cadherin ectodomain and its cDNA clone. We thank also the members of the Carrión-Vázquez laboratory for discussion and critical reading of the manuscript. Financial support from the "Fundación Ramón Areces" to the Centro de Biología Molecular is also acknowledged.

REFERENCES

1. Hynes, R. O. (1999) *Trends Cell Biol.* **9,** M33–M37
2. Vogel, V., and Sheetz, M. (2006) *Nat. Rev. Mol. Cell Biol.* **7,** 265–275
3. Schwartz, M. A., and DeSimone, D. W. (2008) *Curr. Opin. Cell Biol.* **20,** 551–556
4. Carrión-Vázquez, M., Oberhauser, A. F., Díez, H., Hervás, R., Oroz, J., Fernández, J., and Martínez-Martín, D. (2006) in *Advanced Techniques in Biophysics* (Arrondo, J. L. R., and Alonso, L., eds) pp. 163–245, Springer-Verlag, Berlin
5. Takeichi, M. (1990) *Annu. Rev. Biochem.* **59,** 237–252
6. Tepass, U., Truong, K., Godt, D., Ikura, M., and Peifer, M. (2000) *Nat. Rev. Mol. Cell Biol.* **1,** 91–100
7. Conacci-Sorrell, M., Zhurinsky, J., and Ben-Ze'ev, A. (2002) *J. Clin. Investig.* **109,** 987–991
8. Yagi, T., and Takeichi, M. (2000) *Genes Dev.* **14,** 1169–1180
9. Pérez-Moreno, M., Jamora, C., and Fuchs, E. (2003) *Cell* **112,** 535–548
10. Yamada, S., Pokutta, S., Drees, F., Weis, W. I., and Nelson, W. J. (2005) *Cell* **123,** 889–901
11. Abe, K., and Takeichi, M. (2008) *Proc. Natl. Acad. Sci. U.S.A.* **105,** 13–19
12. Kim, S. H., Li, Z., and Sacks, D. B. (2000) *J. Biol. Chem.* **275,** 36999–37005
13. Noren, N. K., Niessen, C. M., Gumbiner, B. M., and Burridge, K. (2001) *J. Biol. Chem.* **276,** 33305–33308
14. Kovacs, E. M., Goodwin, M., Ali, R. G., Paterson, A. D., and Yap, A. S. (2002) *Curr. Biol.* **12,** 379–382
15. Braga, V. M. (2002) *Curr. Opin. Cell Biol.* **14,** 546–556
16. Ko, K. S., Arora, P. D., and McCulloch, C. A. (2001) *J. Biol. Chem.* **276,** 35967–35977
17. Chu, Y. S., Thomas, W. A., Eder, O., Pincet, F., Perez, E., Thiery, J. P., and Dufour, S. (2004) *J. Cell Biol.* **167,** 1183–1194
18. Lamprecht, R., and LeDoux, J. (2004) *Nat. Rev. Neurosci.* **5,** 45–54
19. Tzima, E., Irani-Tehrani, M., Kiosses, W. B., Dejana, E., Schultz, D. A., Engelhardt, B., Cao, G., DeLisser, H., and Schwartz, M. A. (2005) *Nature* **437,** 426–431
20. Müller, U. (2008) *Curr. Opin. Cell Biol.* **20,** 557–566
21. Ganz, A., Lambert, M., Saez, A., Silberzan, P., Buguin, A., Mège, R. M., and Ladoux, B. (2006) *Biol. Cell* **98,** 721–730
22. Brieher, W. M., Yap, A. S., and Gumbiner, B. M. (1996) *J. Cell Biol.* **135,** 487–496
23. Boggon, T. J., Murray, J., Chappuis-Flament, S., Wong, E., Gumbiner, B. M., and Shapiro, L. (2002) *Science* **296,** 1308–1313
24. He, W., Cowin, P., and Stokes, D. L. (2003) *Science* **302,** 109–113
25. Hewat, E. A., Durmort, C., Jacquamet, L., Concord, E., and Gulino-Debrac, D. (2007) *J. Mol. Biol.* **365,** 744–751
26. Zhang, Y., Sivasankar, S., Nelson, W. J., and Chu, S. (2009) *Proc. Natl. Acad. Sci. U.S.A.* **106,** 109–114
27. Troyanovsky, R. B., Klingelhöfer, J., and Troyanovsky, S. (1999) *J. Cell Sci.* **112,** 4379–4387
28. Chappuis-Flament, S., Wong, E., Hicks, L. D., Kay, C. M., and Gumbiner, B. M. (2001) *J. Cell Biol.* **154,** 231–243
29. Baumgartner, W., Hinterdorfer, P., Ness, W., Raab, A., Vestweber, D., Schindler, H., and Drenckhahn, D. (2000) *Proc. Natl. Acad. Sci. U.S.A.* **97,** 4005–4010
30. Baumgartner, W., Golenhofen, N., Grundhöfer, N., Wiegand, J., and Drenckhahn, D. (2003) *J. Neurosci.* **23,** 11008–11014
31. Zhu, B., Chappuis-Flament, S., Wong, E., Jensen, I. E., Gumbiner, B. M., and Leckband, D. (2003) *Biophys. J.* **84,** 4033–4042
32. Sivasankar, S., Zhang, Y., Nelson, W. J., and Chu, S. (2009) *Structure* **17,** 1075–1081
33. Harrison, O. J., Bahna, F., Katsamba, P. S., Jin, X., Brasch, J., Vendome, J., Ahlsen, G., Carroll, K. J., Price, S. R., Honig, B., and Shapiro, L. (2010) *Nat. Struct. Mol. Biol.* **17,** 348–357
34. Ciatto, C., Bahna, F., Zampieri, N., VanSteenhouse, H. C., Katsamba, P. S., Ahlsen, G., Harrison, O. J., Brasch, J., Jin, X., Posy, S., Vendome, J., Ranscht, B., Jessell, T. M., Honig, B., and Shapiro, L. (2010) *Nat. Struct. Mol. Biol.* **17,** 339–347
35. Sotomayor, M., Weihofen, W. A., Gaudet, R., and Corey, D. P. (2010) *Neuron* **66,** 85–100
36. Elledge, H. M., Kazmierczak, P., Clark, P., Joseph, J. S., Kolatkar, A., Kuhn, P., and Müller, U. (2010) *Proc. Natl. Acad. Sci. U.S.A.* **107,** 10708–10712
37. Giannone, G., Mège, R. M., and Thoumine, O. (2009) *Trends Cell Biol.* **19,** 475–486
38. Ladoux, B., Anon, E., Lambert, M., Rabodzey, A., Hersen, P., Buguin, A., Silberzan, P., and Mège, R. M. (2010) *Biophys. J.* **98,** 534–542
39. Wiest, M. C., Eagleman, D. M., King, R. D., and Montague, P. R. (2000) *J. Neurophysiol.* **83,** 1329–1337

40. Pokutta, S., Herrenknecht, K., Kemler, R., and Engel, J. (1994) *Eur. J. Biochem.* **223,** 1019–1026
41. Alattia, J. R., Ames, J. B., Porumb, T., Tong, K. I., Heng, Y. M., Ottensmeyer, P., Kay, C. M., and Ikura, M. (1997) *FEBS Lett.* **417,** 405–408
42. Koch, A. W., Pokutta, S., Lustig, A., and Engel, J. (1997) *Biochemistry* **36,** 7697–7705
43. Pertz, O., Bozic, D., Koch, A. W., Fauser, C., Brancaccio, A., and Engel, J. (1999) *EMBO J.* **18,** 1738–1747
44. Häussinger, D., Ahrens, T., Sass, H. J., Pertz, O., Engel, J., and Grzesiek, S. (2002) *J. Mol. Biol.* **324,** 823–839
45. Choi, Y. S., Sehgal, R., McCrea, P., and Gumbiner, B. M. (1990) *J. Cell Biol.* **110,** 1575–1582
46. Ginsberg, D., DeSimone, D., and Geiger, B. (1991) *Development* **111,** 315–325
47. Sotomayor, M., and Schulten, K. (2008) *Biophys. J.* **94,** 4621–4633
48. Tai, C. Y., Kim, S. A., and Schuman, E. M. (2008) *Curr. Opin. Cell Biol.* **20,** 567–575
49. Rader, C., and Sonderegger, P. (1999) in *Ig Superfamily Molecules in the Nervous System* (Sonderegger, P., ed) pp. 1–22, Harwood Academic Publishers, Amsterdam
50. Harpaz, Y., and Chothia, C. (1994) *J. Mol. Biol.* **238,** 528–539
51. Shapiro, L., Kwong, P. D., Fannon, A. M., Colman, D. R., and Hendrickson, W. A. (1995) *Proc. Natl. Acad. Sci. U.S.A.* **92,** 6793–6797
52. Li, H., Oberhauser, A. F., Redick, S. D., Carrión-Vázquez, M., Erickson, H. P., and Fernández, J. M. (2001) *Proc. Natl. Acad. Sci. U.S.A.* **98,** 10682–10686
53. Steward, A., Toca-Herrera, J. L., and Clarke, J. (2002) *Protein Sci.* **11,** 2179–2183
54. Miroux, B., and Walker, J. E. (1996) *J. Mol. Biol.* **260,** 289–298
55. Sambrook, J., and Russell, D. (1989) *Molecular Cloning: A Laboratory Manual*, 3rd Ed., Cold Spring Harbor Laboratory Press, Cold Spring Harbor, NY
56. Bers, D. M., Patton, C. W., and Nuccitelli, R. (1994) *Methods Cell Biol.* **40,** 3–29
57. Valbuena, A., Oroz, J., Hervás, R., Vera, A. M., Rodríguez, D., Menéndez, M., Sulkowska, J. I., Cieplak, M., and Carrión-Vázquez, M. (2009) *Proc. Natl. Acad. Sci. U.S.A.* **106,** 13791–13796
58. Florin, E. L., Rief, M., Lehmann, H., Ludwig, M., Dornmair, C., Moy, V. T., and Gaub, H. E. (1995) *Biosens. Bioelectron.* **10,** 895–901
59. Bustamante, C., Marko, J. F., Siggia, E. D., and Smith, S. (1994) *Science* **265,** 1599–1600
60. Marko, J. F., and Siggia, E. D. (1995) *Macromolecules* **28,** 8759–8770
61. Case, D. A., Pearlman, D. A., Caldwell, J. W., Cheatham, T. E., III, Wang, J., Ross, W. S., Simmerling, C. L., Darden, T. A., Merz, K. M., Stanton, R. V., Cheng, A. L., Vincent, J. J., Crowley, M., Tsui, V., Gohlke, H., Radmer, R. J., Duan, Y., Pitera, J., Massova, I., Seibel, G. L., Singh, U. C., Weiner, P. K., and Kollman, P. A. (2002) *AMBER7*, University of California, San Francisco
62. Bradbrook, G. M., Gleichmann, T., Harrop, S. J., Habash, J., Raftery, J., Kalb (Gilboa), A. J., Yariv, J., Hillier, I. H., and Helliwell, J. R. (1998) *J. Chem. Soc. Faraday Trans.* **94,** 1603–1611
63. Tsui, V., and Case, D. A. (2000) *Biopolymers* **56,** 275–291
64. Weiser, J., Shenkin, P. S., and Still, W. C. (1999) *J. Comput. Chem.* **20,** 217–230
65. Humphrey, W., Dalke, A., and Schulten, K. (1996) *J. Mol. Graph.* **14,** 33–38, 27–28
66. Ainavarapu, S. R., Brujic, J., Huang, H. H., Wiita, A. P., Lu, H., Li, L., Walther, K. A., Carrión-Vázquez, M., Li, H., and Fernández, J. M. (2007) *Biophys. J.* **92,** 225–233
67. Prasad, A., and Pedigo, S. (2005) *Biochemistry* **44,** 13692–13701
68. Prasad, A., Zhao, H., Rutherford, J. M., Housley, N., Nichols, C., and Pedigo, S. (2006) *Proteins* **62,** 111–121
69. Ainavarapu, S. R., Li, L., Badilla, C. L., and Fernández, J. M. (2005) *Biophys. J.* **89,** 3337–3344
70. Cao, Y., Yoo, T., and Li, H. (2008) *Proc. Natl. Acad. Sci. U.S.A.* **105,** 11152–11157
71. Junker, J. P., Ziegler, F., and Rief, M. (2009) *Science* **323,** 633–637
72. Arias-Moreno, X., Cuesta-Lopez, S., Millet, O., Sancho, J., and Velázquez-Campoy, A. (2010) *Proteins* **78,** 950–961
73. Ozawa, M., Engel, J., and Kemler, R. (1990) *Cell* **63,** 1033–1038
74. Bayas, M. V., Schulten, K., and Leckband, D. (2004) *Mech. Chem. Biosyst.* **1,** 101–111
75. Cailliez, F., and Lavery, R. (2006) *Biophys. J.* **91,** 3964–3971
76. Lu, H., and Schulten, K. (1999) *Proteins* **35,** 453–463
77. Sotomayor, M., Corey, D. P., and Schulten, K. (2005) *Structure* **13,** 669–682
78. Lee, E. H., Hsin, J., Sotomayor, M., Comellas, G., and Schulten, K. (2009) *Structure* **17,** 1295–1306
79. Salt, A. N., Inamura, N., Thalmann, R., and Vora, A. (1989) *Am. J. Otolaryngol.* **10,** 371–375
80. Brown, E. M., Vassilev, P. M., and Hebert, S. C. (1995) *Cell* **83,** 679–682
81. Maurer, P., and Hohenester, E. (1997) *Matrix Biol.* **15,** 569–581
82. Breitwieser, G. E. (2008) *Int. J. Biochem. Cell Biol.* **40,** 1467–1480
83. Rusakov, D. A., Kullmann, D. M., and Stewart, M. G. (1999) *Trends Neurosci.* **22,** 382–388
84. Brusés, J. L. (2006) *Mol. Neurobiol.* **33,** 237–252
85. Oberhauser, A. F., Marszalek, P. E., Erickson, H. P., and Fernández, J. M. (1998) *Nature* **393,** 181–185
86. Evans, E., and Ritchie, K. (1999) *Biophys. J.* **76,** 2439–2447
87. Panorchan, P., Thompson, M. S., Davis, K. J., Tseng, Y., Konstantopoulos, K., and Wirtz, D. (2006) *J. Cell Sci.* **119,** 66–74
88. Bajpai, S., Feng, Y., Krishnamurthy, R., Longmore, G. D., and Wirtz, D. (2009) *J. Biol. Chem.* **284,** 18252–18259
89. le Duc, Q., Shi, Q., Blonk, I., Sonnenberg, A., Wang, N., Leckband, D., and de Rooij, J. (2010) *J. Cell Biol.* **189,** 1107–1115
90. del Río, A., Pérez-Jiménez, R., Liu, R., Roca-Cusachs, P., Fernández, J. M., and Sheetz, M. P. (2009) *Science* **323,** 638–641
91. Kazmierczak, P., Sakaguchi, H., Tokita, J., Wilson-Kubalek, E. M., Milligan, R. A., Müller, U., and Kachar, B. (2007) *Nature* **449,** 87–91
92. Schwander, M., Xiong, W., Tokita, J., Lelli, A., Elledge, H. M., Kazmierczak, P., Sczaniecka, A., Kolatkar, A., Wiltshire, T., Kuhn, P., Holt, J. R., Kachar, B., Tarantino, L., and Müller, U. (2009) *Proc. Natl. Acad. Sci. U.S.A.* **106,** 5252–5257
93. Shin, J. B., and Gillespie, P. G. (2009) *Proc. Natl. Acad. Sci. U.S.A.* **106,** 4959–4960